INL/CON-07-12103
PREPRINT

Test Results of High Temperature Steam/CO_2 Co-electrolysis in a 10-Cell Stack

American Nuclear Society Embedded Topical International Meeting on Safety and Technology of Nuclear Hydrogen Production, Control, and Management

Carl M. Stoots
James E. O'Brien
Joseph J. Hartvigsen

June 2007

The INL is a
U.S. Department of Energy
National Laboratory
operated by
Battelle Energy Alliance

TEST RESULTS OF HIGH TEMPERATURE STEAM/CO_2 COELECTROLYSIS IN A 10-CELL STACK

Carl M. Stoots, James E. O'Brien

Idaho National Laboratory
Idaho Falls, Idaho 83415-3890
carl.stoots@inl.gov

Joseph J. Hartvigsen

Ceramatec, Inc.
Salt Lake City, UT 84119
jjh@ceramatec.com

ABSTRACT

High temperature coelectrolysis experiments with CO_2 / H_2O mixtures were performed in a 10-cell planar solid oxide stack. Results indicated that stack apparent ASR values were shown not to vary significantly between pure steam electrolysis and steam / CO_2 coelectrolysis values. Product gas compositions measured via an online micro gas chromatograph (GC) showed excellent agreement to predictions obtained from a chemical equilibrium coelectrolysis model developed for this study. Experimentally determined open cell potentials and thermal neutral voltages for coelectrolysis compared favorably to predictions obtained from a chemical equilibrium coelectrolysis and energy balance model, also developed for this study.

I. INTRODUCTION

Worldwide, the demand for light hydrocarbon fuels such as gasoline and diesel oil is increasing. To satisfy this demand, oil companies have begun to utilize oil deposits of lower hydrogen content (e.g., Athabasca Oil Sands). Although there is no immediate danger of a world oil supply crisis, world oil production will peak within the next few decades. It is therefore appropriate that oil alternatives be explored and developed. Furthermore, such alternatives may reduce domestic dependence upon foreign oil and sensitivity to oil price volatility.

For the long term, the United States is exploring the feasibility of a hydrogen-based energy economy, with the goals of reduced oil consumption, foreign energy independence, and reduced greenhouse gas emissions. However, since hydrogen is an energy carrier and not an energy source, attaining these goals is conditional upon development of suitable renewable energy sources and/or nuclear power for carbon-free hydrogen production. Furthermore, the conversion process to a hydrogen-based energy economy will require decades.

An interim solution and bridge to a hydrogen economy are synthetically-derived hydrocarbon fuels (synfuels). Synfuel production is a mature technology and, with the price of oil hovering near $70 / barrel, synfuel production has become economical as well. The raw material for synfuel production is syngas – a mixture of hydrogen (H_2) and carbon monoxide (CO). Traditionally, syngas has been produced via coal gasification, and more recently by steam reforming of natural gas, both techniques of which consume non-renewables and emit greenhouse gases.

The Idaho National Laboratory (INL), in conjunction with Ceramatec Inc. (Salt Lake City, USA), has initiated an experimental / computational research program investigating a novel technique for producing syngas which does not consume non-renewables or emit greenhouse gases (Refs. 1, 2). This program entails using nuclear energy to power reversible solid-oxide fuel cells, electrolyzing steam and carbon dioxide (CO_2) simultaneously (Eq. 1):

$$H_2O + CO_2 \longrightarrow H_2 + CO + O_2 . \qquad (1)$$

Coelectrolysis, however, is significantly more complex than simple steam electrolysis. This is primarily due to the multiple reactions that occur: steam electrolysis, CO_2 electrolysis, and the reverse shift reaction (RSR):

$$CO_2 + H_2 \leftrightarrow CO + H_2O. \qquad (2)$$

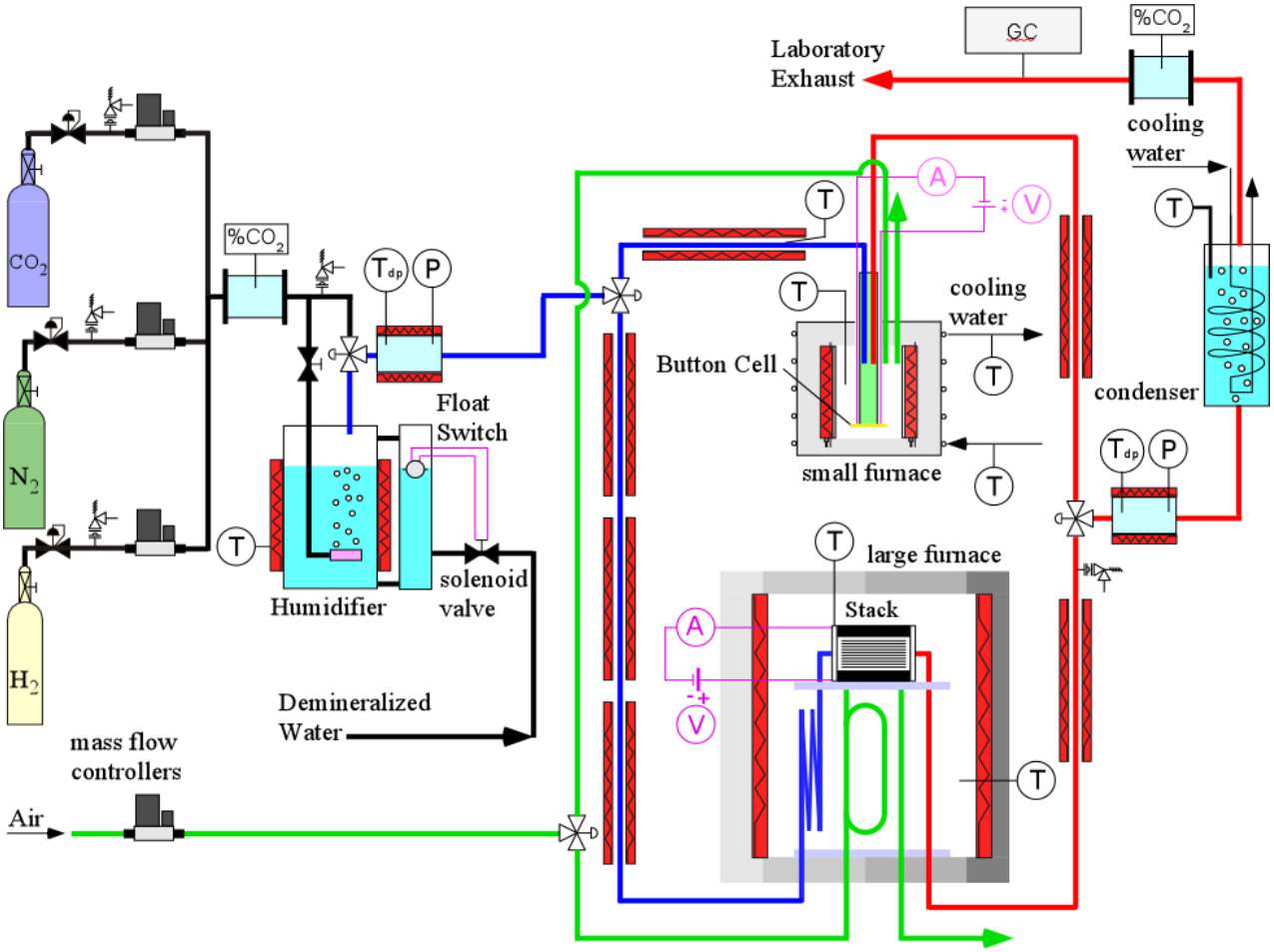

Fig. 1. Schematic of INL coelectrolysis test apparatus.

Reaction kinetics govern the relative contributions of these three reactions. It is also important to note that the electrolysis reactions are not equilibrium reactions. The electrolyte separates the products from the reactants. However, the RSR is a kinetically fast, equilibrium reaction at high temperature in the presence of a Ni catalyst. Also, if the cell potential is high enough, CO can be further electrolyzed to elemental C:

$$CO \rightarrow C + \frac{1}{2} O_2 \qquad (3)$$

producing solid particulates that can then deposit on cell surfaces and reduce cell performance. At temperatures below 700°C, catalytic (Ni) formation of methane may occur (Refs. 3, 4):

$$CO + 3H_2 \rightarrow CH_4 + H_2O \qquad (4)$$

Finally, there could be material compatibility issues related to corrosion and seal leakage.

Syngas could be produced more simply via separate electrolysis of steam and CO_2. There are, however, significant advantages to electrolyzing steam and CO_2 simultaneously. Focusing only upon the electrolysis step, coelectrolysis is more energy efficient than separate electrolysis. For a given solid oxide electrolysis cell, CO_2 electrolysis will exhibit a higher area specific resistance (ASR) than for steam electrolysis. This is due to the slower overall kinetics of CO_2 electrolysis and the higher overpotentials required. In coelectrolysis, the reverse gas shift reaction is relied upon for most of the CO production and therefore the overall electrical requirement is less. A second advantage is that in coelectrolysis the likelihood of producing carbon by electrolysis of CO is reduced.

Results of CO_2 / H_2O electrolysis experiments performed to date in a 10-cell planar solid oxide stack are presented and discussed. These results include electrolysis performance at various temperatures, gas mixtures, and electrical settings. Product gas compositions, as measured via an online micro gas chromatograph (GC), are compared to predictions obtained from a chemical equilibrium/electrolysis model. Better understanding of the feasibility of producing syngas using high temperature electrolysis may initiate

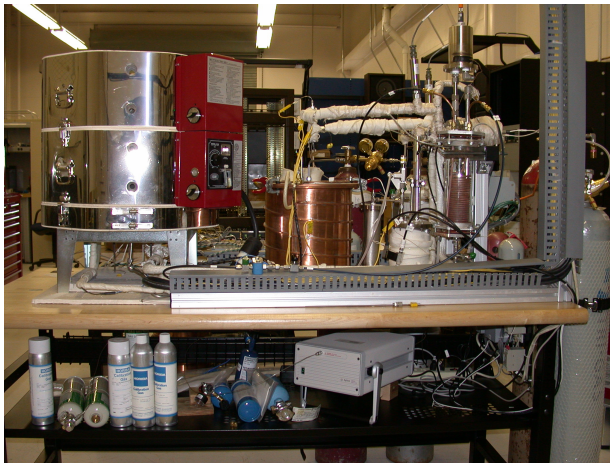

Fig. 2. Photograph of the INL coelectrolysis

the systematic investigation of nuclear-powered synfuel production as a bridge to the future hydrogen economy and ultimate independence from foreign energy resources (Ref. 4).

II. DESCRIPTION OF TEST FACILITY

A schematic of the apparatus used for co-electrolysis testing at the INL is shown in Figure 1. A photograph of the test hardware follows in Figure 2. Primary components include gas supply cylinders, mass-flow controllers, a humidifier, dewpoint measurement stations, carbon dioxide concentration measurement stations, microchannel gas chromatograph, temperature and pressure measurement, high temperature furnace, and a solid oxide electrolysis cell. Nitrogen is used as an inert carrier gas. The use of a carrier gas allows for independent variation of both the partial pressures and the flow rates of the inlet steam, hydrogen, and CO_2 gases while continuing to operate near atmospheric pressure. The flow rates of nitrogen, hydrogen and air are established by means of precision mass-flow controllers. Air flow to the stack is supplied by the shop air system, after passing through a two-stage extractor / dryer unit.

Downstream of the mass-flow controllers, nitrogen is mixed with smaller flows of hydrogen gas and CO_2. Hydrogen is included in the inlet flow as a reducing gas in order to prevent oxidation of the Nickel cermet electrode material. The nitrogen / hydrogen / CO_2 gas mixture is mixed with steam by means of a heated humidifier. The humidifier water temperature is maintained at a constant setpoint value using computerized feedback control. The dewpoint temperature of the nitrogen / hydrogen / CO_2 / steam gas mixture exiting the humidifier is monitored continuously using a precision dewpoint sensor. Pressure is also measured at the dewpoint measurement stations using absolute pressure transducers. Local stream pressure information is required to determine the mole fraction of steam in the gas mixture at the dew point

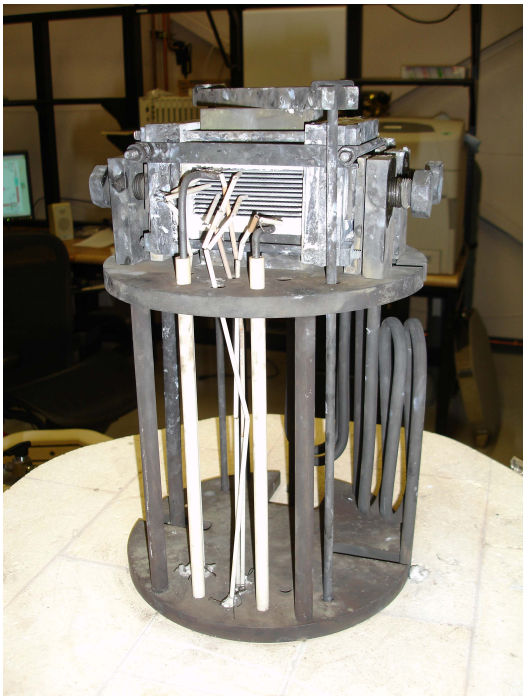

Fig. 3. 10-cell stack mounted on test fixture on furnace base, ready to test.

measurement station. These measurements have indicated that the dewpoint temperature of the gas mixture leaving the humidifier is very close to the water bath temperature, but not necessarily equal to it. Inlet CO_2 concentration is also monitored using an infrared CO_2 sensor. Since the vapor pressure of the water and the resulting partial pressure of the steam exiting the humidifier are determined by the water bath temperature, the water vapor mass flow rate is directly proportional to the carrier gas flow rate for a specified bath temperature. Also, since the nitrogen, hydrogen, and CO_2 flow rates are fixed by the mass flow controllers, and the steam partial pressure is fixed by the bath temperature, the complete inlet gas composition is precisely known at all times. All gas lines located downstream of the humidifier are heat-traced in order to prevent steam condensation. Gas line temperatures are monitored by thermocouples and controlled by means of computer-controlled SCRs.

The inlet gas mixture is then directed to the high temperature furnace (Skutt Model KS818-3), capable of producing temperatures up to 1250°C, which heats and maintains the electrolyzer at the appropriate test temperature via computer-based feedback control. The furnace also preheats the inlet gas mixture and the air sweep gas. A photograph of the stack, mounted on its inconel test fixture and resting on the furnace base, is shown in Fig. 3. The power leads are inconel rods insulated with alumina tubing. The steam /hydrogen / CO_2 and air sweep inlet tubes are coiled to provide additional length for heat transfer upstream of the stack.

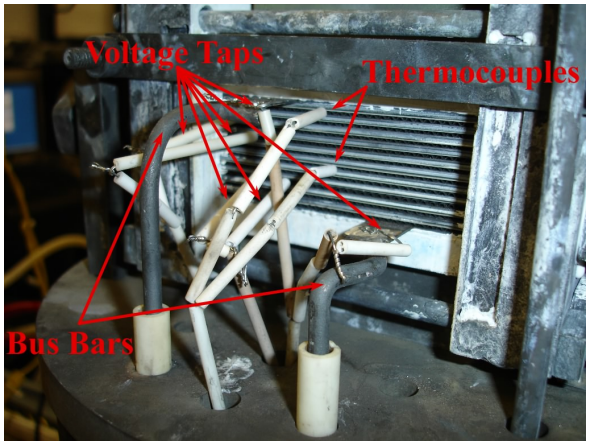

Fig. 4. Close-up of 10-cell stack, showing intra-cell thermocouples, voltage leads, and power leads.

Coelectrolysis testing was performed in the temperature range of 800–830°C.

The stack was fabricated by Ceramatec, Inc., of Salt Lake City, UT. This stack has a per-cell active area of 64 cm^2, for a total active area of 640 cm^2. It is designed to operate in cross flow, with the steam /hydrogen / CO_2 gas mixture entering the inlet manifold on the right side in the photograph (Fig. 3), and exiting through the outlet manifold, visible on the left (Fig. 3). Airflow enters at the rear though an air inlet manifold, not visible in Fig. 3, and exits at the front directly into the furnace.

Fig. 4 is a close-up of the 10-cell stack air outlet plane, showing the miniature intra-cell thermocouples, voltage taps, and power lead bus bars. The power lead attachment tabs are integral with the upper and lower interconnect plates. Stack operating voltages were measured using wires that were directly spot-welded onto these tabs. Four intermediate cell voltages were monitored using small diameter wires inserted into the airflow channels. In addition, two miniature thermocouples were inserted into the airflow channels to monitor internal stack temperatures. These were inconel-sheathed, 0.020 in. (500 μm) OD, mineral-insulated, ungrounded, type-K thermocouples. Thermocouple #1 was located centrally on the top cell (cell #1) and thermocouple #2 was located centrally on the sixth cell from the top.

The internal components of the stack are comprised as follows. The interconnect plate is fabricated primarily from ferritic stainless steel. It includes an impermeable separator plate (~0.46 mm thick) with edge rails and two corrugated "flow fields," one on the sweep-gas side and one on the steam / hydrogen / CO_2 side. The height of the flow channel formed by the edge rails and flow fields is 1.0 mm. Each flow field includes 32 perforated flow channels across its width to provide uniform gas-flow distribution. The steam / hydrogen / CO_2 flow field is fabricated from nickel foil. The sweep flow field is ferritic stainless steel. The interconnect plates and flow fields also serve as electrical conductors and current distributors. To improve performance, the sweep-side separator plates and flow fields are surface - treated to form a rare-earth conductive oxide scale. A perovskite rare-earth coating is also applied to the separator-plate oxide scale by either screen printing or plasma spraying. On the steam / hydrogen / CO_2 side of the separator plate, a thin (~10 μm) nickel metal coating is applied.

The electrolyte is scandia-stabilized zirconia, ~140 μm thick. The sweep-side electrode (anode in the electrolysis mode) is a strontium-doped manganite. The electrode is graded, with an inner layer of manganite/zirconia (~13 μm) immediately adjacent to the electrolyte, a middle layer of manganite (~18 μm), and an outer bond layer of cobaltite. The steam / hydrogen / CO_2 electrode (cathode in the electrolysis mode) is also graded, with a nickel cermet layer (~13 μm) immediately adjacent to the electrolyte and a pure nickel outer layer (~10 μm).

The syngas product stream exiting the furnace is directed towards a second dewpoint sensor and a CO_2 sensor upon exiting the furnace and then to a condenser through a heat-traced line. The condenser removes most of the residual steam from the exhaust. The final exhaust stream is vented outside the laboratory through the roof.

The rates of steam and CO_2 electrolysis are measured via three different, independent methods: 1) electrical current through the stack, 2) the measured change in inlet and outlet steam and CO_2 concentrations as measured by the on-line dew point and CO_2 sensors, and 3) an on-line microchannel GC. The GC also tests for any additional electrolysis products, such as CH_4, that may be produced.

Some additional discussion of the test apparatus, experimental procedures, data reduction, and the stack construction may be found in Ref. 5.

III. DESCRIPTION OF MODEL

To understand the impact of the electrolysis reactions and the RSR discussed above, and to assist with interpretation of experimentally measured data, a chemical equilibrium coelectrolysis model was developed. This model also served to help determine the necessary inlet conditions for the range of experiments that were conducted. Using a correlation for the reverse gas shift reaction equilibrium constant as a function of gas temperature and the room temperature inlet gas molar composition, the model calculates the equilibrium gas composition as the inlet gas mixture heats up to electrolysis conditions (800 to 830°C).

The open-cell potential for the coelectrolysis system can be calculated as a function of temperature using the Nernst equation for either steam-hydrogen or for CO_2-CO, provided the equilibrium composition of the components is used in the evaluating the equation. Therefore, the equilibrium composition must be

determined first, by any appropriate method. Our coelectrolysis chemical equilibrium model determines the equilibrium composition of the system as follows.

The overall shift reaction can be represented as:

$$a_0 + b_0 + c_0 + d_0 \rightarrow a_1 + b_1 + c_1 + d_1 \quad (5)$$

where a_0, b_0, c_0, and d_0 represent the cold inlet mole fractions of CO, CO_2, H_2, and H_2O, respectively, that are known from the inlet gas flow rate and dewpoint measurements. The unknown equilibrium mole fractions of the four species at the electrolyzer temperature, prior to electrolysis, are represented by a_1, b_1, c_1, and d_1. The three corresponding chemical balance equations for carbon, hydrogen, and oxygen are:

$$a_0 + b_0 = a_1 + b_1 \quad (6)$$

$$2c_0 + 2d_0 = 2c_1 + 2d_1 \quad (7)$$

$$a_0 + 2b_0 + d_0 = a_1 + 2b_1 + d_1. \quad (8)$$

To complete a system of four equations and four unknowns, the equilibrium constant for the shift reaction:

$$k_{RSR}(T) = \frac{b_1 c_1}{a_1 d_1} \quad (9)$$

is included.

Once the hot equilibrium composition is determined, the Nernst potential can be calculated from:

$$V_N = \frac{-\Delta G_{f,H_2O}(T)}{2F} - \frac{RT}{2F}\ln\left[\left(\frac{d_1}{c_1 y_{O2}^{1/2}}\right)\left(\frac{P}{P_{std}}\right)^{-1/2}\right] = \frac{-\Delta G_{f,CO_2}(T)}{2F} - \frac{RT}{2F}\ln\left[\left(\frac{d_1}{c_1 y_{O2}^{1/2}}\right)\left(\frac{P}{P_{std}}\right)^{-1/2}\right] \quad (10)$$

where $\Delta G_{f,H2O}$ and $\Delta G_{f,CO2}$ are the Gibbs free energy of formation for H_2O and CO_2, R is the ideal gas constant, and y_{O2} is the mole fraction of oxygen on the sweep side of the cells ($y_{O2} \sim 0.21$).

The electrolyzer outlet composition can be determined similarly, with one exception. The chemical balance equation for oxygen must be modified to account for the electrolytic reduction of the CO_2/steam mixture. Accordingly, the oxygen balance equation becomes:

$$a_1 + 2b_1 + d_1 = a_2 + 2b_2 + d_2 + \Delta n_O \quad (11)$$

where Δn_O is the relative molar rate of oxygen removal from the CO_2 / steam mixture, give by:

$$\Delta n_O = \frac{IN_{cells}}{2F\dot{N}_{Tot,fuel}}. \quad (12)$$

In this equation, I is the electronic current, N_{cells} is the total number of cells in the stack, and $\dot{N}_{Tot,fuel}$ is the total molar flow rate on the CO_2/steam side, including any inert gas flows. So the post-electrolyzer equilibrium composition (state 2) can be determined again from simultaneous solution of three chemical balance equations and the equilibrium constant equation.

The model was verified by comparing results with experimental results for various electrolysis current values, inlet compositions, and electrolysis temperatures.

IV. DISCUSSION OF RESULTS

To assess the feasibility of high temperature co-electrolysis for syngas production, as well as test the accuracy of the coelectrolysis chemical equilibrium model developed at the INL, a 10-cell planar stack was tested under coelectrolysis conditions (Figs. 3 and 4). Several different sets of inlet compositions and operating temperatures were studied (Table 1).

Cell ASR is dependent upon the type of electrolysis being conducted, with pure CO_2 electrolysis exhibiting a significantly higher ASR than steam electrolysis (Ref. 1). However, in coelectrolysis the RSR is relied upon for most CO_2-to-CO conversion, and steam electrolysis is the primary electrolytic reaction. Therefore, there is little change in ASR from steam electrolysis to coelectrolysis. To demonstrate this, polarization curves were generated

TABLE 1. Summary of test conditions.

Test #	$T_{furnace}$ (C)	Flow Rates			Inlet Dew Point (C)	Molar Composition			
		H_2 (sccm)	CO_2 (sccm)	N_2 (sccm)		H_2 (mol %)	CO_2 (mol %)	N_2 (mol %)	H_2O (mol %)
0	800	497	0	3010	51.5	12.0	0	72.6	15.4
1	800	497	605	3010	51.5	10.2	12.4	61.9	15.5
2	800	497	505	2510	45.5	12.6	12.7	63.3	11.4
3	800	497	705	1010	66.0	15.6	22.2	31.8	30.4
4	800	497	756	3010	74.0	6.7	10.1	40.2	43.0
5	828	497	605	3011	51.5	10.2	12.4	61.9	15.5
6	828	497	756	3513	65.3	7.3	11.2	52.0	29.5

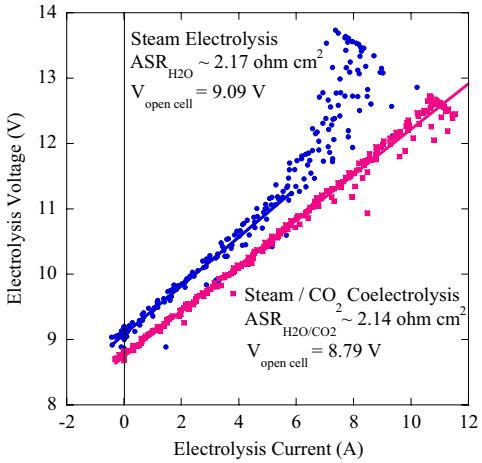

Fig. 5. Polarization curves for steam electrolysis and coelectrolysis, with mean ASR values.

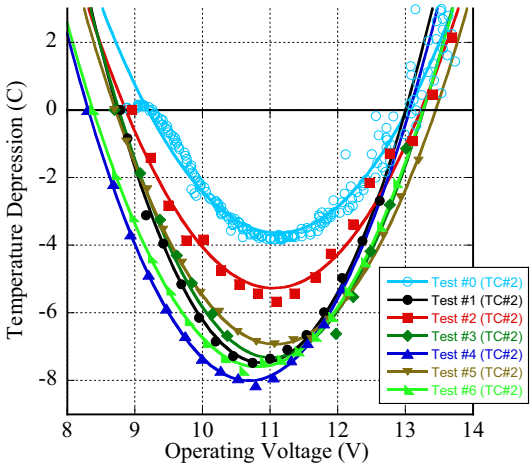

Fig. 6. Internal stack temperature (thermocouple #2) for various test conditions.

for the 10-cell stack for steam electrolysis and H_2O/CO_2 coelectrolysis. Once the stack was at the operating temperature of 800°C, a steam electrolysis polarization curve was generated by performing a voltage sweep for the conditions labeled "Test #0" in Table 1. This same voltage sweep was repeated for the coelectrolysis conditions "Test #1". These results are shown in Figure 5. Using these data, the sweep-average apparent ASR was calculated by numerically averaging the voltage and current data:

$$ASR = \sum \frac{1}{n} \frac{(V_{op} - V_{OC}) / N_{cells}}{I / A_{cell}} \qquad (13)$$

where n is the number of measurements included, V_{op} is the operating voltage, V_{oc} is the measured open cell potential, and A_{cell} is the active area of each cell (64 cm^2). Steam electrolysis sweep data above 6 A current exhibited a large amount of scatter, possibly due to local steam starvation, and was not included in the apparent ASR calculations. The straight lines represent linear fits of the data. There was almost no change in apparent ASR for coelectrolysis versus steam electrolysis, reinforcing the hypothesis that steam electrolysis is the principal electrolysis reaction and that the RSR is mostly responsible for CO production.

Figure 6 presents internal stack temperature depression (the difference between the temperature measured during the sweep and the temperature at open cell conditions) for thermocouple #2 as a function of stack operating voltage for the 7 electrolysis conditions listed in Table 1. Steam electrolysis, CO_2 electrolysis, and the RSR are endothermic reactions that tend to depress the cell temperature during electrolysis. However, the cell ohmic heating tends to increase the cell temperature, proportional to the square of the current. These two effects balance each other at the thermal neutral voltage. At operating voltages below thermal neutral, the endothermic heat of reaction dominates and the cell temperature is lower than that at open cell. At operating voltages above thermal neutral, ohmic heating dominates and the cell temperature will exceed that at open cell. For pure steam electrolysis, the thermal neutral voltage is a weak function of temperature only and is equal to 1.287 V at 800°C and 1.288 V at 830°C. For coelectrolysis, however, the thermal neutral voltage is also a function of gas composition. By curve fitting the experimental data (shown as lines in Figure 6) and solving for zero temperature depression, experimental thermal neutral voltages were estimated. Experimental open cell potentials were directly measured. To predict the theoretical open cell potentials and thermal neutral voltages, the chemical equilibrium coelectrolysis model discussed above was extended to include an energy balance. This more complex model is discussed in Ref. 6. Table 2 summarizes the measured versus predicted open cell potentials and thermal neutral voltages for the experimental conditions listed in Table 1. The average difference between measured and predicted thermal neutral voltages for the 6 coelectrolysis tests conducted was 17 mV.

TABLE 2. Comparison of measured versus predicted open cell potentials and thermal neutral voltages.

Test #	Open Cell Potential (volts per cell)		Thermal Neutral Voltage (volts per cell)	
	Measured	Predicted	Measured	Predicted
1	0.8795	0.8923	1.3004	1.3437
2	0.8959	0.9082	1.3231	1.3476
3	0.8700	0.8826	1.3271	1.3446
4	0.8392	0.8421	1.3017	1.3161
5	0.8696	0.8803	1.3447	1.3451
6	0.8376	0.8471	1.3265	1.3285

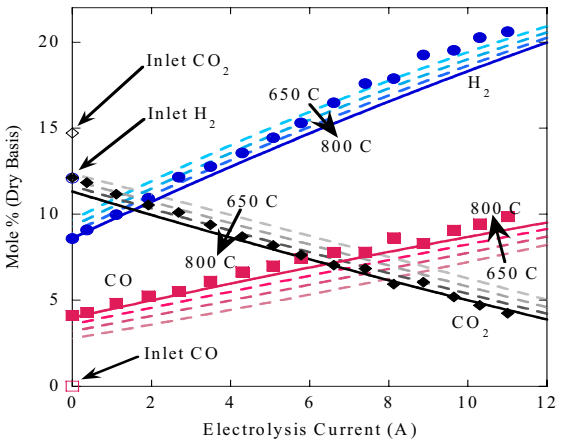

Fig. 7. Effect of varying chemical equilibrium coelectrolysis model equilibrium temperature (Eq. 9) with comparison to Test 1 experimental data..

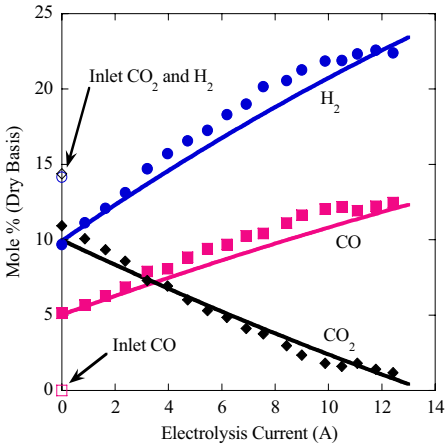

Fig. 8. Test 2 experimental and chemical equilibrium coelectrolysis model results, T_{equil} = 800 C.

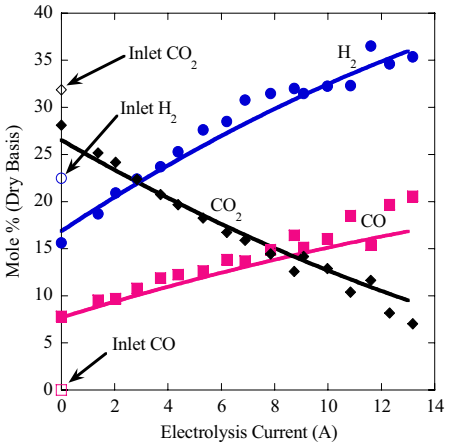

Fig. 9. Test 3 experimental and chemical equilibrium coelectrolysis model results, T_{equil} =800 C.

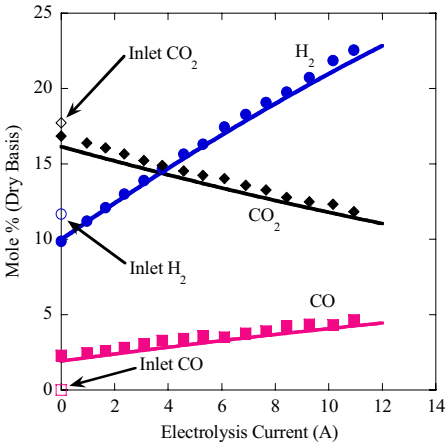

Fig. 10. Test 4 experimental and chemical equilibrium coelectrolysis model results, T_{equil} = 800 C.

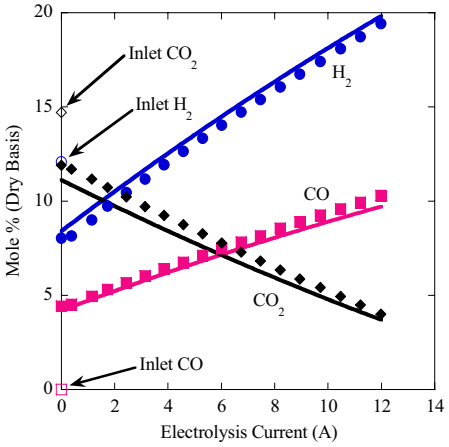

Fig. 11. Test 5 experimental and chemical equilibrium coelectrolysis model results, T_{equil} = 828 C.

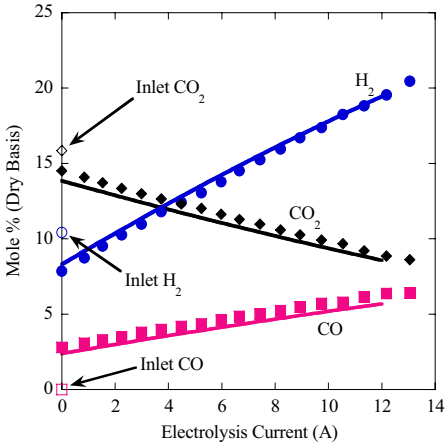

Fig. 12. Test 6 experimental and chemical equilibrium coelectrolysis model results, T_{equil} = 828 C.

Figs. 7-12 present the compositions of steam, CO2, hydrogen, and CO as a function of electrolysis current on a dry basis for tests 1-6. Lines represent various model predictions and symbols represent experimental measurements. The effects of varying the equilibrium temperature used in the chemical equilibrium coelectrolysis model for the conditions of Test #1 are shown in Fig. 7. The RSR equilibrium constant is a function of temperature, as shown in Equation (9). Since product gases cool to room temperature before analysis in the micro GC, it was not certain what value to use for an "apparent" equilibrium temperature for the products. Therefore, the chemical equilibrium coelectrolysis model was run for several different equilibrium temperatures ranging from 650°C to 800°C. It was found that setting the chemical equilibrium coelectrolysis model equilibrium temperature equal to the furnace temperature produced the best comparisons, indicating that the products are kinetically frozen after they leave the hot zone, probably due to lack of any significant catalyst surface and the cool-down is fairly rapid. Predicted compositions were therefore evaluated at the electrolyzer temperature for all subsequent evaluations (Figures 8 through 12).

Figures 7 through 12 demonstrate that even at zero current there was a drop in CO_2 and H_2 mole fractions from the cold inlet values, with CO produced. This is solely due to the RSR. As the electrolysis current was increased, the yield of syngas increased linearly while the concentration of CO_2 (and H_2O, not shown in the figures) decreased. These figures also show overall good agreement between experimental GC data and results from the chemical equilibrium coelectrolysis model for the range of testing performed in this study. Finally, in the case of Test #6, at the maximum current studied the product H_2 concentration was doubled and product CO_2 concentration was reduced to half that of the process inlet mixture.

V. CONCLUSIONS

The INL has been conducting an experimental and modeling study to assess the feasibility and performance of high temperature solid oxide cells operated in an electrolysis mode for simultaneous coelectrolysis of H_2O and CO_2 for syngas production. Results presented in this paper were obtained from a 10-cell planar electrolysis stack, with an active area of 64 cm^2 per cell. The stack was operated over a temperature range of 800 to 830°C. Inlet gas compositions as well as electrical current were also varied. Stack apparent ASR values were shown not to vary significantly between pure steam electrolysis and steam / CO_2 coelectrolysis. Product gas compositions were measured via an online micro gas chromatograph (GC) and showed good comparison to predictions obtained from a chemical equilibrium coelectrolysis model developed at the INL. Experimentally determined thermal neutral voltages for coelectrolysis were compared to an enhanced chemical equilibrium coelectrolysis model, also developed at the INL. Better understanding of the feasibility of producing syngas using high temperature electrolysis may initiate the systematic investigation of nuclear-powered synfuel production as a bridge to the future hydrogen economy and ultimate independence from foreign energy resources.

NOMENCLATURE

a, b, c, d	mole fractions CO, CO_2, H_2, and H_2O respectively
A_{cell}	active area of each cell, cm^2
ASR	apparent area specific resistance, Ohm cm^2
F	Faraday's constant, 96487 J/V mol
ΔG_f	Gibbs free energy of formation, J/mol
I	total electronic current, A
k_{RSR}	Reverse Shift Reaction equilibrium constant
n	number of measurements
Δn_0	relative molar rate of oxygen removal from the CO_2/steam side, mol/s
N_{cells}	total number of cells in the stack
$\dot{N}_{Tot,fuel}$	total molar flow rate on CO_2/steam side of cells, mol/s
P	pressure, Pa
P_{std}	standard pressure, Pa
R	universal gas constant, J/mol K
T	temperature, K
V_N	Nernst potential, V
V_{OC}	stack open cell potential, V
V_{op}	stack operating voltage, V
y	mole fraction

ACKNOWLEDGMENTS

This work was supported by the Idaho National Laboratory, Laboratory Directed Research and Development program and the U.S. Department of Energy, Office of Nuclear Energy, Nuclear Hydrogen Initiative Program.

REFERENCES

1. C.M. Stoots, J.E. O'Brien, G.L. Hawkes, J.S. Herring, and J.J. Hartvigsen, "High Temperature Co-Electrolysis of H2O and CO2 for Syngas Production," *2006 Fuel Cell Seminar*, Honolulu, Hawaii, Nov. 13-17, 2006, paper no. 418.
2. G.L. Hawkes, J.E. O'Brien, C.M. Stoots, R. Jones, "Three Dimensional CFD Model of a Planar Solid Oxide Electrolysis Cell for Co-Electrolysis of Steam and Carbon-Dioxide," *2006 Fuel Cell Seminar*, Honolulu, Hawaii, Nov. 13-17, 2006, paper no. 298.

3. S.H. Jensen, J.V.T. Høgh, R. Barfod, M. Mogensen, "High temperature electrolysis of steam and carbon dioxide," In *Energy technologies for Post Kyoto targets in the medium term,* Proceedings of *Risø International Energy Conference*, Risø, Denmark, May 19-21, 2003.
4. S. H. Jensen, and M. Mogensen, "Perspectives of High Temperature Electrolysis Using SOEC," *19th World Energy Congress 2004*, Sydney, Australia, September 5-9, 2004.
5. J.E. O'Brien, C.M. Stoots, and J.Hartvigsen, "Hydrogen Production Performance of a 10-Cell Planar Solid-Oxide Electrolysis Stack," *Journal of Fuel Cell Science and Technology*, **3**, 1 (May 2006).
6. J.E. O'Brien, C.M. Stoots, G.L. Hawkes, J.S. Herring, and J.Hartvigsen, "High-Temperature Co-electrolysis of Carbon Dioxide and Steam for the Production of Syngas; Equilibrium Model and Single-Cell Tests," *Safety and Technology of Nuclear Hydrogen Production, Control and Management (ST-NH2), Embedded Topical Meeting, ANS Annual Meeting*, June 24-28, 2007 (accepted).